Polymer 51 (2010) 1853–1860

Contents lists available at ScienceDirect

Polymer

journal homepage: www.elsevier.com/locate/polymer

# Computer simulation study on the shear-induced phase separation in semi-dilute polymer solutions by using Ianniruberto–Marrucci model

Shotaro Nishitsuji [a], Mikihito Takenaka [b,*], Takashi Taniguchi [c]

[a] Graduate School of Science and Engineering, Yamagata University, Yonezawa 992-8510, Japan
[b] Department of Polymer Chemistry, Graduate School of Engineering, Kyoto University, Kyoto 615-8510, Japan
[c] Department of Chemical Engineering, Graduate School of Engineering, Kyoto University, Kyoto 615-8510, Japan

ARTICLE INFO

*Article history:*
Received 22 November 2009
Received in revised form
18 February 2010
Accepted 18 February 2010
Available online 26 February 2010

*Keywords:*
Shear-induced phase separation
Doi–Onuki thoery
Ianniruberto–Marrucci model

ABSTRACT

In our previous study, a computer simulation scheme based on Doi–Onuki theory is proposed to simulate the dynamics of the shear-induced phase separation in semi-dilute polymer solutions [KOBUNSHI RONBUNSHU 2007, 64, 324]. The scheme employs Ianniruberto–Marrucci model as a constitutive equation to express the viscoelastic behavior of the solution explicitly. The scheme enables us to simulate the time-evolution of stress as well as that of shear-induced structure upon shear-jump. In this study, we focus on the conformation of polymer chains. The dynamics of the polymer chains agrees with those in the "solvent squeeze" model which interprets the shear-induced phase separation phenomena in semi-dilute polymer solutions by Saito et al. [Macromolecules **1999**, 32, 4879].



## 1. Introduction

When shear flow is imposed to a semi-dilute polymer solution in its one phase region, the solution exhibits strong turbidity. Ver Strade and Philippoff [1] firstly found this phenomenon in polystyrene(PS)/dioctyl phthalate(DOP) and PS/decaline solution under the shear flow in a capillary tube. Since then, many experimental and theoretical studies on the phenomenon have been done in order to understand the phenomenon called the shear-induced phase separation. Wu et al. [2] investigated the shear-induced structure of PS/DOP by light scattering and found that the scattering intensity was enhanced in the first and third quadrants of $q_x$–$q_y$ plane, where $\mathbf{q} = (q_x,q_y,q_z)$ is the scattering vector and $x$, $y$, and $z$ direction are, respectively, the flow direction, the velocity gradient direction and the neutral direction. The unique scattering pattern for the shear-induced structure is called "butterfly pattern".

The scattering pattern in $q_x$–$q_z$ plane for the shear-induced structure of the semi-dilute polymer solutions has been also observed by light scattering [3–7] and small angle neutron scattering [8,9]. In $q_x$–$q_z$ plane, the butterfly patterns where the scattering intensity increases along $q_x$-axis have been found. Kume et al. [7] investigated time-evolution of stress and concentration fluctuations upon shear-jump by means of both flow light scattering and rheological measurement for PS/DOP. The butterfly pattern appeared in light scattering of $q_x$–$q_z$ plane upon shear-jump and the peak positions of the butterfly pattern shifted to small angle with time according to the coarsening of the phase-separated structure under shear flow. In the time-evolution of stress, several overshoots due to growth of the phase-separated structures were found in addition to the first overshoot associating with disentanglement.

In theoretical studies, Helfand and Fredrickson(HF) [10] firstly developed a dynamical equation of the concentration fluctuations, which accounts for shear-induced phase separation in polymer solution. The equation includes the gradient term of the stress tensor is incorporated into Ginzburg–Landau type free energy functional. Subsequently, Doi and Onuki proposed two fluid model [11]. In this model, the nonlinear term of HF theory is included. The computer simulation of the shear-induced phase separation with the two fluid model has been firstly done by Onuki et al. [12,13]. Subsequently, Okuzono [14] numerically studied the dynamics of the shear-induced phase separation and the time-evolution of rheology of polymer solution under shear flow in two dimensional space on a basis of two fluid model by using Smoothed-particle hydrodynamics method. Furukawa and Onuki [15] observed the chaotic behavior in shear-induced phase separation phenomena at higher shear rate. In all simulation, the structure factors of the phase-separated structures under shear flow exhibit the butterfly patterns with the peaks in the first and third quadrants of $q_x$–$q_y$ plane as experimentally observed by Wu et al. [2]. Our group [16] has simulated the time-evolution of concentration fluctuations

* Corresponding author. Tel.: +81 75 383 2622; fax: +81 75 383 2623.
*E-mail address:* takenaka@alloy.polym.kyoto-u.ac.jp (M. Takenaka).

0032-3861/$ – see front matter © 2010 Elsevier Ltd. All rights reserved.
doi:10.1016/j.polymer.2010.02.031

and stress upon shear-jump in three dimensional spaces by using the two fluid model with the similar condition to Kume's experiments [7]. In our simulation, the concentration fluctuations were enhanced and the butterfly pattern was observed in $q_x$–$q_z$ plane as well as $q_x$–$q_y$ plane as observed experimentally, indicating that the simulation can well describe the behaviors of the concentration fluctuations of the polymer solution under shear flow. However the stress observed in our simulation increased monotonically and then became constant, and did not show any overshoot behaviors observed in the experiment by Kume. The discrepancy in the behavior of stress between our simulation and experiment originates from the usage of Maxwell model as constitutive equation in our simulation. It is well known that Maxwell model employed in our simulation cannot describe the nonlinear viscoelasticity of the solution correctly [16]. Subsequently, we developed a computer simulation scheme to simulate the behavior of the mechanical properties of the solution exhibiting shear-induced phase separation well, as well as the time-evolution of the concentration fluctuations [17]. In order to express the viscoelastic behaviors of the semi-dilute polymer solutions correctly, we incorporated the Ianniruberto–Marrucci(IM) model [18–20] instead of Maxwell model to the two fluid model as a constitutive equation. The IM model includes i) entangled chains relaxation by reputation, ii) constraint release (both thermal and convective), and iii) stretch relaxation (include the effect of upper limited stretch), and was found to be able to describe the viscoelastic behaviors of polymer solutions well. In this study, we focus on the conformation of polymer chains which is characterized by the chain stretch rate and the orientation of segments.

The contents of this paper are as follows: In Section 2, we will describe the detail of the simulation scheme of the time dependent Ginzburg–Landau type equation with IM model, where the effects of concentration fluctuations are included. In Section 3, we will show the results of the simulation, and the characteristic of the simulation results. Finally we will conclude our results in Section 4.

## 2. Simulation scheme

According to the two fluid model [11], the change in the volume fraction of polymer $\phi$ with time $t$ is expressed by

$$\left(\frac{\partial}{\partial t}+\mathbf{v}\cdot\nabla\right)\phi = \nabla\cdot\left[L\left(\nabla\mu-\frac{1}{\phi}\nabla\cdot\boldsymbol{\sigma}_{\mathrm{p}}\right)\right]+\nabla\cdot\mathbf{J}, \tag{1}$$

where $\mathbf{v}$ is the velocity field, $L$ is the Onsager kinetic coefficient, $\mu$ is the chemical potential, $\boldsymbol{\sigma}_{\mathrm{p}}$ is the stress tensor and $\mathbf{J}$ is the thermal noise. The chemical potential is given by [21]

$$\mu = \frac{k_BT}{a^3}\left[\frac{1}{N}\ln\phi+\frac{1}{N}-\ln(1-\phi)-1+\chi(1-2\phi) -\frac{a^2}{18\phi(1-\phi)}\nabla^2\phi\right], \tag{2}$$

where $k_B$ is the boltzmann coefficient, $T$ is the absolute temperature, $a$ is the statistical segment length of the polymer, $N$ is the polymerization index, and $\chi$ is the Flory–Huggins interaction parameter per monomer. $L$ is given by [22,23]

$$L = \frac{a^2}{6\pi\eta_0} \tag{3}$$

with $\eta_0$ being the viscosity of solvent. The velocity field follows the Stokes equation under the incompressible condition:

$$\eta_0\nabla^2\mathbf{v}-\nabla p-\phi\nabla\mu+\nabla\cdot\boldsymbol{\sigma}_{\mathrm{p}} = 0, \tag{4}$$

with $p$ being pressure.

According to the fluctuation dissipation theorem [24], $J_i$ satisfies

$$\left\langle J_i(\mathbf{r},t)J_j(\mathbf{r}',t')\right\rangle = 2k_BTL\delta(\mathbf{r}-\mathbf{r}')\delta(t-t')\delta_{ij}. \tag{5}$$

As described before, IM model describing the viscoelastic behaviors of the solutions includes reputation, constraint release (both thermal and convective), and stretch relaxation with the effect of upper limited stretch.

According to IM model [18–20], the stress tensor is given by

$$\boldsymbol{\sigma}_{\mathrm{p}} = G(\phi)\mathbf{S}\lambda^2\frac{\lambda_{\max}-1}{\lambda_{\max}-\lambda}, \tag{6}$$

where $G(\phi)$ is the plateau modulus in a semi-dilute polymer solution at $\phi$, $\mathbf{S}$ is the tensor of the average tube orientation, $\lambda$ is the stretch ratio and $\lambda_{\max}$ is upper limit of stretch ratio. The factors including $\lambda$ in Equation (6) describes the stretch relaxation. The concentration dependence of the plateau modulus $G(\phi)$) is expressed by [25]

$$G(\phi) = G\phi^{2.3} \tag{7}$$

with $G$ being the plateau modulus in bulk of polymer. The time-evolution of $\mathbf{S}$ is given by

$$\frac{\partial T_{ij}}{\partial t} = -(\mathbf{v}_p\cdot\nabla)T_{ij}+\frac{\partial v_{pi}}{\partial x_k}T_{kj}+T_{ik}\frac{\partial v_{pj}}{\partial x_k}-2T_{ij}(\mathbf{K}:\mathbf{S}) -\frac{2}{\tau}\left(T_{ij}-\frac{1}{3}S_{ij}\right), \tag{8}$$

$$\mathbf{T} = \mathbf{S}^2, \mathbf{K}:\mathbf{S} = \sum_i\sum_j k_{ij}S_{ji} = Tr(\mathbf{kS}),$$

where $\mathbf{v}_{\mathrm{p}}$ is the velocity field of polymer, $\mathbf{k}$ is the velocity gradient tensor, and $\tau$ is the relaxation time of tube segment. $\mathbf{v}_{\mathrm{p}}$ is given by [11]

$$\mathbf{v}_p = \mathbf{v}+\frac{L}{\phi}\left(-\nabla\mu+\frac{1}{\phi}\nabla\cdot\boldsymbol{\sigma}_{\mathrm{p}}\right). \tag{9}$$

$\tau$ is given by

$$\tau = \frac{1}{2\left(\frac{1}{\tau_d(\phi)}+|\mathbf{k}:\mathbf{S}|\right)}+\tau_R(\phi), \tag{10}$$

where $\tau_{\mathrm{d}}(\phi)$ and $\tau_R(\phi)$ are the reptation time of a semi-dilute polymer solution and the Rouse time of a semi-dilute polymer solution at $\phi$, respectively. Equation (10) includes the effects of constraint release. The concentration dependence of $\tau_{\mathrm{d}}(\phi)$ and $\tau_R(\phi)$ is expressed by [25–27]

$$\tau_d(\phi) = \tau_d\phi^{2.8} \tag{11}$$

and

$$\tau_R(\phi) = \tau_R\phi^{1.0}, \tag{12}$$

where $\tau_{\mathrm{d}}$ and $\tau_R$ are, respectively, the reptation time and the Rouse time in bulk of polymer. The time evolution of $\lambda$ is given by

$$\frac{\mathrm{d}\lambda}{\mathrm{d}t} = \lambda\mathbf{k}:\mathbf{S}-\frac{\lambda_{\max}}{\tau_R(\phi)}\frac{\lambda-1}{\lambda_{\max}-\lambda}. \tag{13}$$

Here, we numerically solve the above equations (1)–(13) on a 256 × 256 square lattice. The $x$ and $y$ axes of the lattice are defined as the flow and the velocity gradient directions, respectively. To apply the shear flow to the system in the simulations, we used the coordinate transform method [28]. In the method, we deformed space coordinates $\mathbf{r} = (x, y)$ at $t_0$ to $\mathbf{r}' = (x', y')$ by

$$x' = x - \dot{\gamma} t y \tag{14}$$

$$y' = y.$$

at $t_1$, where $t = t_1 - t_0$.

Then, we rewrite the gradient term as

$$\nabla' = \left(\frac{\partial}{\partial x'}, \frac{\partial}{\partial y'} - \gamma\frac{\partial}{\partial x'}\right), \tag{15}$$

so that the deformed Laplacian is

$$\nabla'^2 = \left(\frac{\partial}{\partial x'}\right)^2 + \left(\frac{\partial}{\partial y'} - \gamma\frac{\partial}{\partial x'}\right)^2 \tag{16}$$

with $\gamma = \dot{\gamma} t$ being strain.

The procedure of the application of shear flow with equation (14) is shown schematically in Fig. 1. The lattice is deformed by tilting $y$-axis by a factor of $\gamma$ with $t$ ((a)→(b)→(c) in Fig. 1). When $\gamma$ become 1, the lattice is restored to the original position with the following equations: $x' = x - y$ and $y' = y$ ((c)→(a) in Fig. 1). This process is repeated in the simulation. There are two advantage points in the coordinate transform method in comparison with shifting method [29,30]. One is that the coordinate transform method is free from the errors caused by Lees–Edwards boundary condition used in shifting method along $y$-direction. The schematic diagram of shifting method is shown in Fig. 2. In shifting method, the usual periodic boundary condition is used along $x$-direction. For 2 dimensional matrix of $\phi_{\text{matrix}}(0,0)$–$(255,255)$ used in our simulation, we set $\phi(256,n_y) = \phi(0, n_y)$ and $\phi(-1,n_y) = \phi(255,n_y)$. On the other hand, along $y$-direction or velocity gradient direction, we need to use Lees–Edwards boundary condition to follow shear flow. In Lees–Edwards boundary condition, we also set $\phi(n_x,256) = \phi(n_x,0)$ and $\phi(n_x,-1) = \phi(n_x,255)$. However, the position of $\phi(n_x,256)$ and $\phi(n_x,-1)$ is, respectively, shifted along $x$-direction by 256 $\dot{\gamma} t$ and $-256\dot{\gamma} t$, thus the position of $\phi(n_x,256)$ and $\phi(n_x,-1)$ becomes $(n_x + 256\ \dot{\gamma} t, 256)$ and $(n_x - 256\ \dot{\gamma} t, -1)$, where $d$ is lattice size. Since $x$-value of the position become off-lattice, we have to interpolate the boundary values from the shifted lattice. So that we can not avoid the errors caused by interpolation. On the other hand, the errors do not occur in the coordinate transform method, since periodic boundary condition can be used for both $x$-axis and $y$-axis in the coordinate transform method. The other is that the Fast Fourier

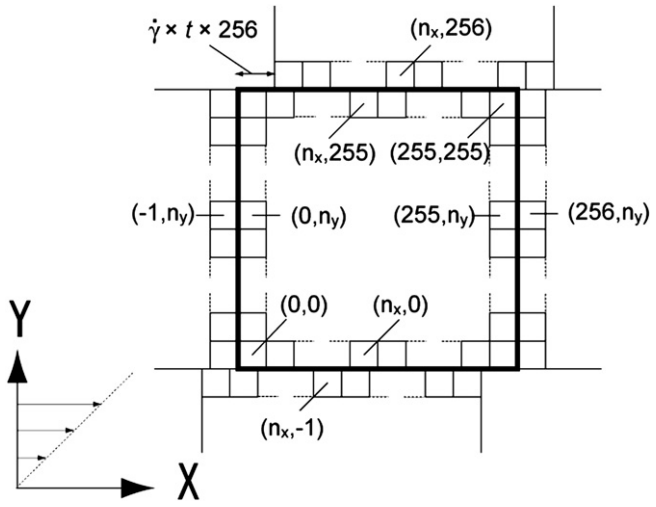


**Fig. 2.** The procedure of the application of shear with the shifting method.

Transform (FFT) can be applied to solve Stokes equation [31] in coordinate transform method while the iteration method has to be used to solve Stokes equation in shifting method. The applicability of FFT results in the reduction of computational time.

We use the following reduced variables for space, time and concentration,

$$\tilde{t} = \frac{t}{t_0}, l = \frac{l}{\xi}, \tilde{\phi} = \frac{\phi}{\phi_c}$$

$$\text{with } \xi = R_g,\ t_0 = \frac{6^{3/2}\pi\eta_0 R_g^3}{k_B T}, \phi_c = \frac{1}{\sqrt{N}+1}. \tag{17}$$

Equations (1), (2), (4), (6) and (8) are respectively reduced to these equations,

$$\left(\frac{\partial}{\partial\tilde{t}} + \tilde{\mathbf{v}}\cdot\tilde{\nabla}\right)\tilde{\phi} = \tilde{\nabla}\cdot\left[\tilde{\nabla}\tilde{\mu} - \frac{1}{\tilde{\phi}}\tilde{\nabla}\cdot\tilde{\sigma}_p\right] + \tilde{\nabla}\cdot\tilde{\mathbf{j}} \tag{18}$$

$$\tilde{\mu} = \mu/\frac{k_B T}{\alpha^3 N} = \left[\ln\tilde{\phi} - \delta\tilde{\chi}\tilde{\phi} + \frac{1}{2}\tilde{\phi}^2 - \frac{1}{3}\frac{1}{\tilde{\phi}}\tilde{\nabla}^2\tilde{\phi}\right],$$
$$\delta\tilde{\chi} = 2N^{1/2}\left(\chi - \frac{1}{2}\right), \tag{19}$$

$$\tilde{\nabla}\tilde{\mathbf{v}} - \tilde{\nabla}\tilde{p} - g\left(\tilde{\phi}\tilde{\nabla}\tilde{\mu} + \tilde{\nabla}\cdot\tilde{\sigma}_p\right) = 0, \tag{20}$$

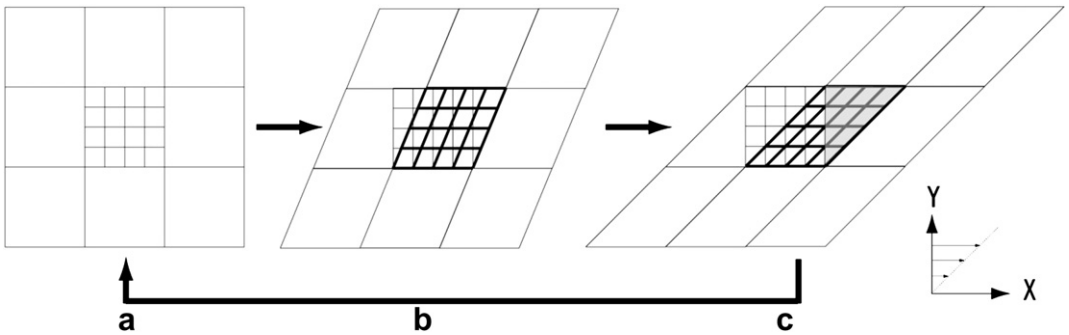


**Fig. 1.** The procedure of the application of shear with the coordinate transform method. The lattice (a) is deformed into (c) up to $t = 1/\dot{\gamma}$. Then right part of the lattice in (c) (shaded region) is moved to left of the lattice.

$$\tilde{\nu} = \nu/\frac{\xi}{t_0},\ \tilde{p} = p/\frac{\eta_0}{t_0},\ g = \frac{\phi_c k_B T}{a^3 N}/\frac{\eta_0}{t_0} = \pi,$$

$$\tilde{\boldsymbol{\sigma}}_p = \boldsymbol{\sigma}_p/\frac{\phi_c k_B T}{a^3 N} = \tilde{G}\tilde{\phi}_0^{2.3}\left(\frac{\tilde{\phi}}{\phi_0}\right)^{2.3}\mathbf{S}\lambda^2\frac{\lambda_{max}-1}{\lambda_{max}-\lambda}, \tag{21}$$

$$\tilde{\tau} = \tau/t_0 = \frac{1}{2\left(\frac{1}{\tilde{\tau}_d\tilde{\phi}_0^{2.8}\left(\frac{\tilde{\phi}}{\phi_0}\right)^{2.8}}\right) + |\tilde{\mathbf{k}}:\mathbf{S}|} + \tilde{\tau}_R\tilde{\phi}_0^{1.0}\left(\frac{\tilde{\phi}}{\tilde{\phi}_0}\right)^{1.0} \tag{22}$$

where $\phi_0$ is the initial volume fraction of polymer. In this study, we used $\delta\tilde{\chi} = 1.38, \tilde{G}\tilde{\phi}_0^{2.3} = 2.5, \tilde{\tau}_d\tilde{\phi}_0^{2.8} = 100.0, \tilde{\tau}_R\tilde{\phi}_0^{1.0} = 0.267$, and $\lambda_{max} = 2.5$. We have set the parameters estimated the experimental condition used in previous experiment of shear-induced phase separation in PS/DOP solution. Thus, the condition of the simulation is the same as the experiment. $\lambda_{max}$ is the same value with the simulation in IM model [20].

## 3. Result and discussion

Fig. 3(a) shows the time-evolution of the concentration fluctuations obtained by the simulation scheme under shear flow with the reduced shear rate $\dot{\tilde{\gamma}} = 0.05$. At $0 < \tilde{t} < 60$, the concentration fluctuations do not seem to change with time. At $60 < \tilde{t}$, the concentration fluctuations grow with time and the string-like domains are formed, the domains then coarsen with time. The time-evolution of the concentration fluctuations shows that shear-induced phase separation occurs under shear flow. On the other hand, under shear flow with $\dot{\tilde{\gamma}} = 0.01$, the concentration fluctuations are not enhanced even at $\tilde{t} = 2000$, as shown in Fig. 3(b). This suggests that critical shear rate for shear-induced phase separation exists between 0.05 and 0.01.

Fig. 4 shows the time changes in the structure factor at $\dot{\tilde{\gamma}} = 0.05$. At $\tilde{t} = 80$, the structure factors start to increase and the peaks in structure factors appear in the first and third quadrants of $q_x$–$q_z$ plane. The peaks then shift toward smaller $\mathbf{q}$ with time. This tendency agrees with the experimental result by Wu [2], indicating that the scheme can simulate the time-evolution of the concentration fluctuations.

First, we focus on the shear rate dependence of shear-induced phase separation. Fig. 5(a) shows time evolution of the spatial average of variance $\overline{\delta\tilde{\phi}}$ at shear rate $\dot{\tilde{\gamma}} = 0.01, 0.04, 0.05$ and 0.1. $\overline{\delta\tilde{\phi}}$ is defined by

$$\overline{\delta\tilde{\phi}} = \sqrt{\left\langle\left(\tilde{\phi}-\tilde{\phi}_0\right)^2\right\rangle}, \tag{23}$$

where $\langle\cdots\rangle$ denotes spatial average. At $\dot{\tilde{\gamma}} = 0.04, 0.05$ and 0.1, the concentration fluctuation increases according to the time-evolution of phase-separated structure under shear flow. On the other hand, $\overline{\delta\tilde{\phi}}$ doesn't increase with time at $\dot{\tilde{\gamma}} = 0.01$. Fig. 5(b) shows the steady-state $\overline{\delta\tilde{\phi}}$ as a function of $\dot{\tilde{\gamma}}$. The discontinuity can be found between 0.025 and 0.04, indicating that the critical shear rate is around 0.03. The terminal linear viscoelastic relaxation time $\tilde{\tau}_w$ is calculated with IM model at $\phi = \phi_0$ found to be 50 in this simulation. According to experimental result [32,33], the critical shear rate and the inverse of the longest relaxation time are, respectively, $3.56 \times 10^{-2}\ s^{-1}$ and $2.08 \times 10^{-2}\ s^{-1}$ for PS/DOP solution at 27 °C and the critical shear rate 0.03 is slightly higher than the inverse of $\tau_w$. The inverse of the longest relaxation time in our simulation is nearly equal to $1/\tilde{\tau}_w = 0.02$, agreeing with the tendency of the experimental results.

Fig. 6 shows $\overline{\delta\tilde{\phi}}$, the spatial averaged shear stress $\tilde{\sigma}_{xy}$ and spatial averaged normal stress difference $\tilde{N}_1$ as functions of time at $\dot{\tilde{\gamma}} = 0.05$(a) and $\dot{\tilde{\gamma}} = 0.01$(b). $\tilde{\sigma}_{xy}$ and $\tilde{N}_1$ are given by

$$\tilde{\sigma}_{xy} = \left\langle\tilde{\sigma}_{pxy}\right\rangle - \left\langle\frac{1}{3\tilde{\phi}}\frac{\partial\tilde{\phi}}{\partial\tilde{x}}\frac{\partial\tilde{\phi}}{\partial\tilde{y}}\right\rangle, \tag{24}$$

and

$$\tilde{N}_1 = \left\langle\tilde{\sigma}_{pxx}-\tilde{\sigma}_{pyy}\right\rangle + \left\langle\frac{1}{3\tilde{\phi}}\left[\left(\frac{\partial\tilde{\phi}}{\partial\tilde{y}}\right)^2-\left(\frac{\partial\tilde{\phi}}{\partial\tilde{x}}\right)^2\right]\right\rangle. \tag{25}$$

In the time evolution of $\tilde{\sigma}_{xy}$ at $\dot{\tilde{\gamma}} = 0.05$, the first overshoot appears around $\tilde{t} = 36$, and then several small overshoots appear. The overshoots were not observed in our previous simulation with Maxwell type constitutive equation (16). The overshoots behaviors agree well with the experimental results by Kume et al. [7], indicating that the new simulation scheme can well simulate not only the shear-induced structure but the stress overshoots behavior. We also plotted the time-evolution of shear stress calculated by using IM model at $\phi_0$ in Fig. 6(a). Although time-evolution of shear stress at $\phi_0$ exhibits the first overshoot, any overshoots don't appear after the first overshoot. Thus, the overshoots after the first overshoot is caused by the shear-induced phase separation. Similar to the behavior of shear stress, the time-evolution of normal stress difference $\tilde{N}_1$ also shows the first large overshoot and several small overshoots after the first overshoot. However $\tilde{N}_1$ calculated with IM model at $\phi_0$, does not exhibits any overshoots. Thus, the overshoots found in the simulation are caused by the shear-induced phase separation. In the case of $\dot{\tilde{\gamma}} = 0.01$(Fig. 6(b)), the shear-induced phase separation doesn't occur, the first small overshoot thus appears in the time evolution of $\tilde{\sigma}_{xy}$ and $\tilde{N}_1$ doesn't show the overshoot behavior. It should be noted that the first terms of equations (24) and (25) are found to be much larger than the second terms arising from the surface tension in two-phase states. Thus $\tilde{\sigma}_{xy} \cong \langle\tilde{\sigma}_{pxy}\rangle$ and $\tilde{N}_1 \cong \langle\tilde{\sigma}_{pxx}-\tilde{\sigma}_{pyy}\rangle$ in this simulation condition, reflecting that the surface tension doesn't contribute to shear stress in two-phase states.

We need to remark the results of the simulation for shear-induced phase separation by Onuki et al. [13]. In the simulation of shear-induced phase separation by Onuki, the stress overshoots have been observed even with Maxwell model, while we cannot find the stress overshoots in our simulation with Maxwell model. This difference is caused by the difference of the conditions in the simulations.

In Onuki's simulation, they set the location of the solution in phase diagram to be very close to critical point and applied strong shear. Under such a condition, the difference of concentration between two phases becomes distinct and the surface tension strongly affects the viscoelastic behaviors. Thus, the overshoots in Onuki's simulation are induced by the deformation of phase boundary not by the viscoelastic properties of the solution described by Maxwell model.

On the other hand, in our previous simulation with Maxwell model, the simulation condition is relatively far from critical point and the shear rate is low since we set the simulation condition to be the same as experimental condition for PS/DOP. With our simulation condition, the effects of surface tension on the viscoelastic properties of the solution are very weak so that the viscoelastic properties of the solution are governed by that of Maxwell model. Thus, we could not observe any overshoots.

In our new simulation with IM model, the overshoots are observed. In our new simulation, we have to consider the first stress overshoot and the stress overshoots after the first overshoot

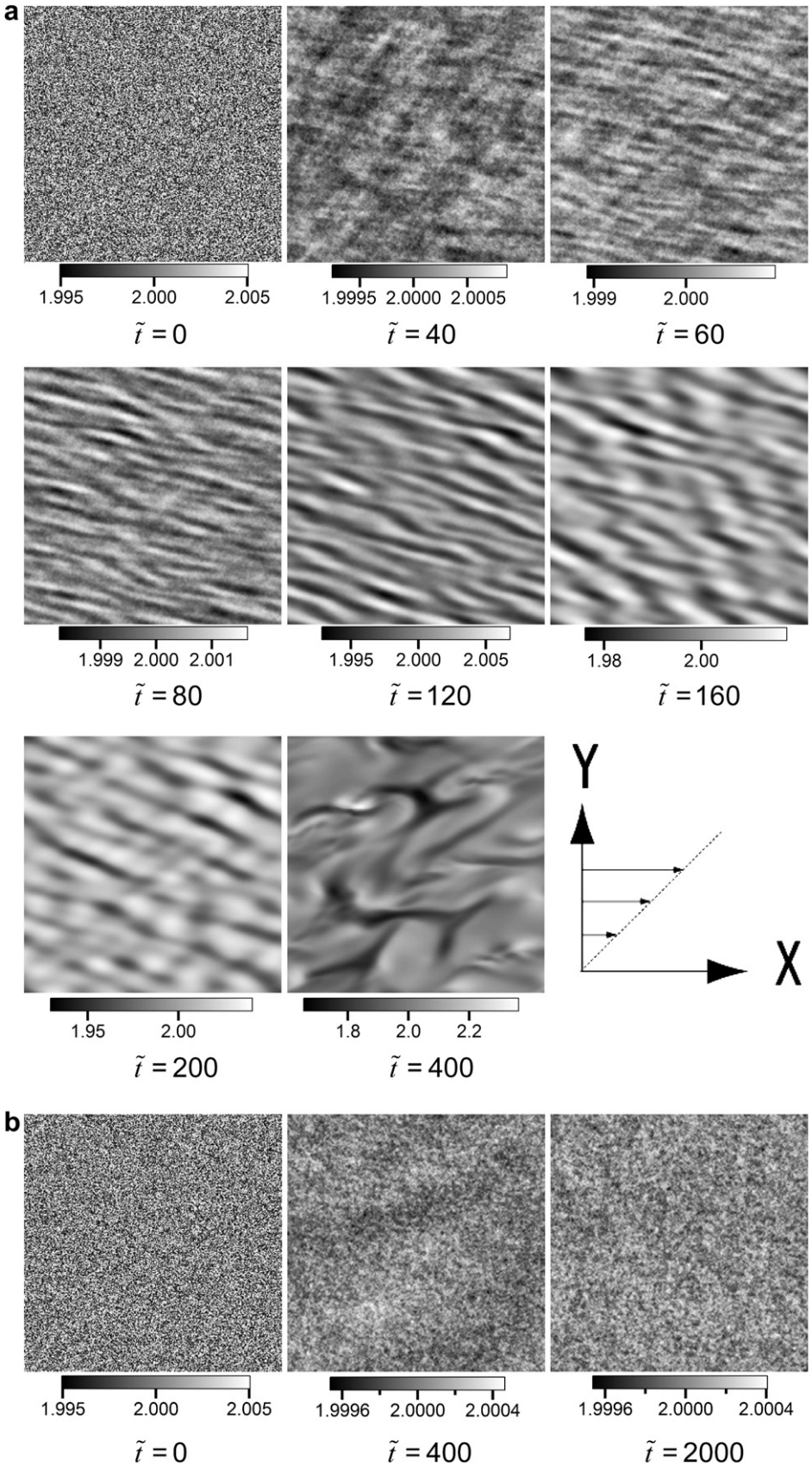


**Fig. 3.** Time changes in the concentration fluctuations with (a) $\tilde{\dot{\gamma}} = 0.05$ and with (b) $\tilde{\dot{\gamma}} = 0.01$.

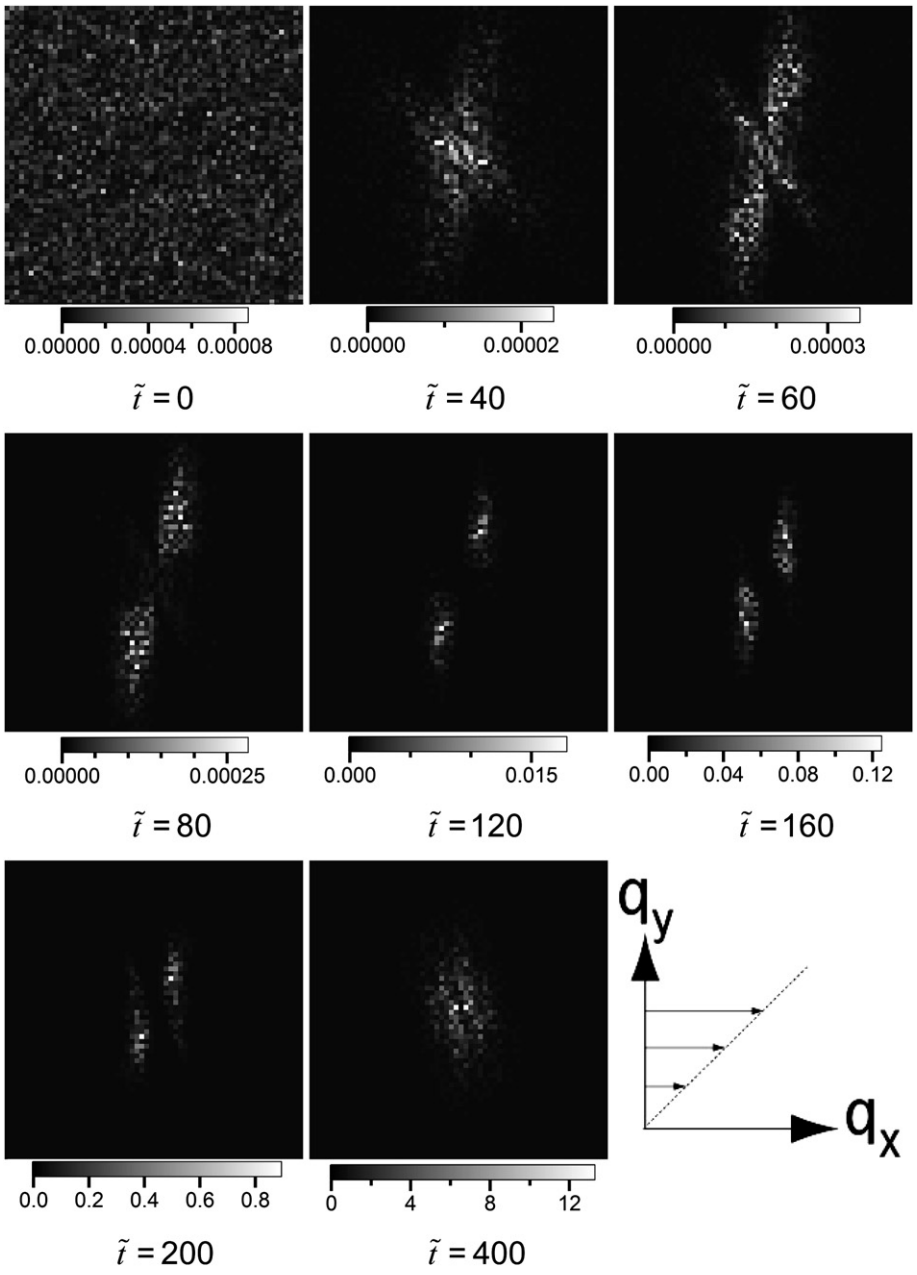


**Fig. 4.** Time changes in the structure factors with $\dot{\tilde{\gamma}} = 0.05$ in $q_x$–$q_y$ plane.

separately, since the origins of the overshoots for each case are different.

As for the first overshoot, IM model is the origin of it. IM model includes the increase in stress due to the orientation and the stretch in polymer chains as well as the decrease by disentanglement so that IM model can exhibit the first stress overshoot even in homogeneous solution. As described previously, in our simulation condition, the viscoelastic properties of the solution are governed by that of the model so that we could observe the first stress overshoot caused by IM model.

As for the stress overshoots after the first stress overshoot, the overshoots originate from the time change in the spatial distribution of the concentration fluctuations induced by shear. The spatial distribution of the concentration fluctuations induces the spatially in homogeneous deformation under shear. The concentration dependence of the viscoelastic properties of IM model is much stronger than that of Maxwell model. Thus, even small amplitude of concentration fluctuations could induce the overshoot with IM model. It should be noted that the origin of our simulation with IM model is different from that of Onuki's simulation with Maxwell model.

Next, we will discuss the change in conformation of polymer chains under shear flow. In the constitutive equations (6)–(13), the conformation can be characterized by the chain stretch rate $\lambda$ and the orientation of segments **S**. Thus, we investigated the increment of $\lambda$, $\delta\lambda$, and the degree of orientation $|\mathbf{a}|/|\mathbf{b}|$, to clarify the time change in conformation under shear-induced phase separation process. Here $\delta\lambda$ is defined as

$$\delta\lambda = \lambda - 1. \tag{26}$$

**a** and **b** are, respectively, the vector of main axis of average tube orientation and that perpendicular to **a**. We also investigated the

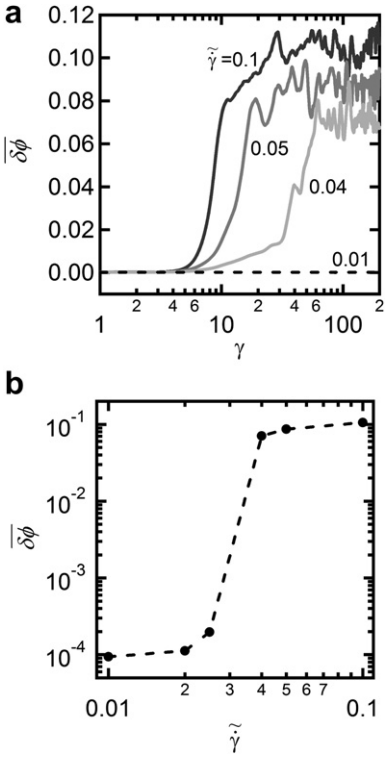


**Fig. 5.** Time-evolution of average variance $\overline{\delta\phi}$ with $\dot{\tilde{\gamma}} = 0.01, 0.04, 0.05, 0.1$ as function of strain γ (a) and the shear rate dependence of $\overline{\delta\phi}$ (b).

angle $\theta$ between **a** and *x*-axis. Fig. 7 shows $\delta\lambda_{conc}$ and $\delta\lambda_{dilute}$ as functions of strain $\gamma$ at $\dot{\tilde{\gamma}} = 0.05$ and $\dot{\tilde{\gamma}} = 0.01$. Here $\delta\lambda_{conc}$ is $\delta\lambda$ averaged in concentrated region at which $\phi$ is larger than $\phi_0$, while $\delta\lambda_{dilute}$ is $\delta\lambda$ averaged in dilute region which $\phi$ is smaller than $\phi_0$. In the case of $\dot{\tilde{\gamma}} = 0.01$, $\delta\lambda$ increases with time at $\gamma < 2$, and then becomes constant at $\gamma > 2$. At $\dot{\tilde{\gamma}} = 0.01$, the entanglements can be well relaxed in the diffusion process of polymer chains so that any overshoot cannot be observed in $\delta\lambda$. On the other hand, in the case of $\dot{\tilde{\gamma}} = 0.05$, we observe the overshoot behaviors due to the entanglements in both $\delta\lambda_{conc}$ and $\delta\lambda_{dilute}$, and the behaviors of $\delta\lambda_{conc}$ and $\delta\lambda_{dilute}$ are identical with $\delta\lambda_0$ calculated with $\phi_0$ at $\gamma < 3$. Since the concentration fluctuation has not been developed at $\gamma < 3$, the solution behaves as homogeneous one and the first overshoot is caused by the remained entanglements. After first overshoot, $\delta\lambda_{conc}$ decreases while $\delta\lambda_{dilute}$ increase with $\gamma$, and the tendency $\delta\lambda_{conc} < \delta\lambda_0 < \delta\lambda_{dilute}$ appears at $\gamma > 3$, reflecting that polymer chains in dilute region are stretched by shear flow.

Fig. 8(a) shows $|\mathbf{a}|/|\mathbf{b}|$ with $\dot{\tilde{\gamma}} = 0.05$ and $\dot{\tilde{\gamma}} = 0.01$, and Fig. 8(b) shows $\theta$ as function of $\gamma$ with $\dot{\tilde{\gamma}} = 0.05$ and $\dot{\tilde{\gamma}} = 0.01$. In the case of $\dot{\tilde{\gamma}} = 0.01$, the behavior of $(|\mathbf{a}|/|\mathbf{b}|)_{conc}$ and $(|\mathbf{a}|/|\mathbf{b}|)_{dilute}$ are identical with that of $(|\mathbf{a}|/|\mathbf{b}|)_{\phi_0}$, and the behavior of $\theta_{dilute}$ and $\theta_{conc}$ is also identical with that of $\theta_{\phi_0}$. On the other hand, in the case of $\dot{\tilde{\gamma}} = 0.05$, before $\overline{\delta\phi}$ increase with $\gamma$ ($\gamma < 5$), $|\mathbf{a}|/|\mathbf{b}|$ increase and $\theta_{dilute}$ and $\theta_{conc}$ decrease with $\gamma$. At $5 < \gamma < 20$ where $\overline{\delta\phi}$ increases with $\gamma$, $|a|/|b|$ decreases and $\theta$ increases gradually in concentrated region, while $|\mathbf{a}|/|\mathbf{b}|$ decreases and $\theta$ decreases slightly in dilute region. Finally, at $20 < \gamma$, both $|\mathbf{a}|/|\mathbf{b}|$ and $\theta$ then fluctuates with time in both regions.

The behaviors of the conformation in polymer chains agree with those in "solvent squeeze" model [34] which explains the shear-induced phase separation phenomena in semi-dilute polymer solutions. The thermal concentration fluctuations in one phase region of the semi-dilute solutions give rise to the inhomogeneity of entanglement density. If we apply the shear flow to the solution, the

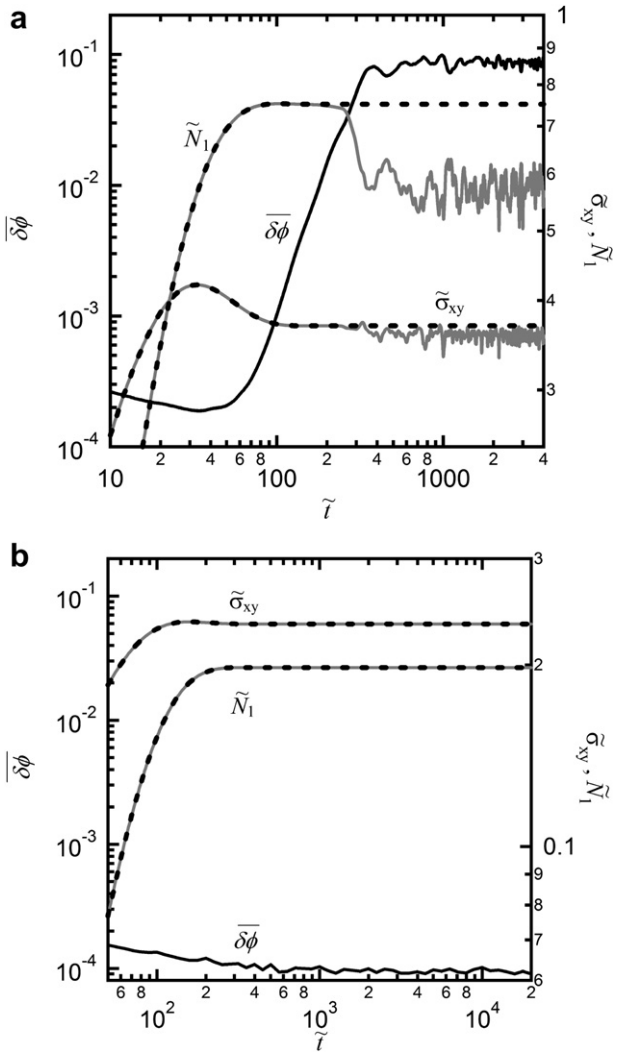


**Fig. 6.** The volume fraction and stress field as functions of time at $\dot{\tilde{\gamma}} = 0.05$ (a) and $\dot{\tilde{\gamma}} = 0.01$ (b). Solid gray lines indicate $\tilde{\sigma}_{xy}$ and $N_1$ with $\tilde{\phi}_0$ respectively.

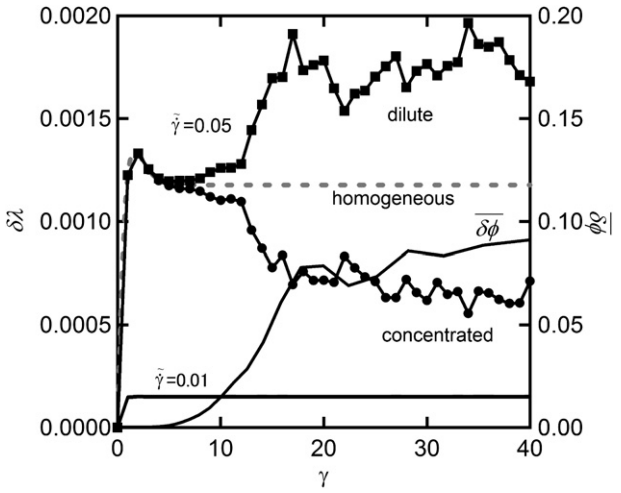


**Fig. 7.** $\delta\lambda_{conc}$ and $\delta\lambda_{dilute}$ as functions of $\gamma$ with $\dot{\tilde{\gamma}} = 0.05$. Filled circles and filled squares indicate $\delta\lambda_{conc}$ in the concentrated region and $\delta\lambda_{dilute}$ in the dilute region with $\dot{\tilde{\gamma}} = 0.05$, respectively. The solid line indicate in both concentrated region and dilute region with $\dot{\tilde{\gamma}} = 0.01$. The broken line indicates $\delta\lambda$ in homogeneous state with $\dot{\tilde{\gamma}} = 0.05$.

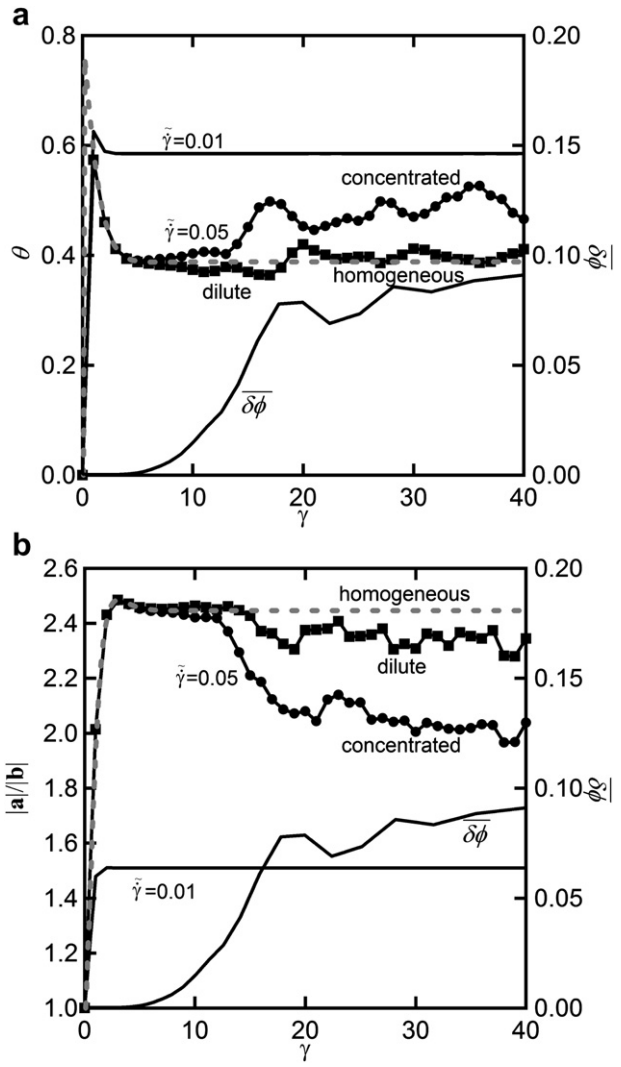


**Fig. 8.** $|\mathbf{a}|/|\mathbf{b}|$ as function of γ (a). Filled circle and filled square indicate $|\mathbf{a}|/|\mathbf{b}|$ in the concentrated region and $|\mathbf{a}|/|\mathbf{b}|$ in the dilute region with $\tilde{\dot{\gamma}} = 0.05$, respectively. The solid line indicate $|\mathbf{a}|/|\mathbf{b}|$ in both concentrated region and dilute region with $\tilde{\dot{\gamma}} = 0.01$. The broken line indicate $|\mathbf{a}|/|\mathbf{b}|$ in homogeneous state with $\tilde{\dot{\gamma}} = 0.05$. $\theta$ as function of $\gamma$ (b). Open circle and filled square indicate $\theta$ in the concentrated region and $\theta$ in the dilute region, respectively. The solid line indicate $\theta$ in both concentrated region and dilute region with $\tilde{\dot{\gamma}} = 0.01$. The broken line indicate $\theta$ in homogeneous state with $\tilde{\dot{\gamma}} = 0.05$.

concentrated region was not deformed well while the dilute region was deformed more than that in the concentrated region. In the case when shear rate is larger than the inverse of terminal relaxation time, the polymer chains cannot relax well by disentanglement. The polymer chain in dilute region is stretched by shear flow and becomes unstable in terms of conformational entropy. In order to relax the unstable stretch, the stretched polymer chains retract toward concentrated region. The retraction enhances the concentration fluctuations and the phase-separated structure is eventually formed under shear flow. As shown in Fig. 7, in the dilute region the polymer chains are stretched and thus dilute region become unstable. However, the concentrated region becomes much stable than the homogeneous solution since the chains are much relaxed. Thus, total free energy of concentrated and dilute regions becomes much lower than that of the homogeneous solution and the concentration fluctuations are kept under shear flow.

In the simulation at $\tilde{\dot{\gamma}} = 0.05$, $\delta\lambda$ and $|\mathbf{a}|/|\mathbf{b}|$ decrease and $\theta$ increases associating with the evolution of concentration fluctuations. These results indicate that the conformation of polymer chains can be relaxed in developing concentrated region, while agrees with the dynamics of polymer chains of the "solvent squeeze" model.

## 4. Conclusion

We developed the new computer simulation scheme based on Doi–Onuki theory, with the Ianniruberto–Marrucci as the constitutive equation, and simulated the shear-induced phase separation with the scheme in two dimensions. The enhancement of the concentration fluctuations occurs under shear flow, the scattering pattern shows so-called "butterfly pattern" and first stress overshoot by disentanglement appeared and some overshoot after the first overshoot can be observed. These results agree with experimental results in terms of structure and mechanical properties. We can characterize the changes in the conformation of polymer chains with time during shear-induced phase separation with $\delta\lambda$, $|\mathbf{a}|/|\mathbf{b}|$, and $\theta$. The time changes in the parameters reflects that the conformation of polymer chains in concentrated region associating with concentration fluctuations, and agrees with the dynamics of the polymer chains in the "solvent squeeze" model.

## References

[1] Ver Strate G, Philippoff WJ. J Polym Sci Polym Lett Ed 1974;12:267.
[2] Wu XL, Pine DJ, Dixon PK. Phys Rev Lett 1991;66:2408.
[3] Hashimoto T, Fujioka K. J Phys Soc Jpn 1991;60:356.
[4] Hashimoto T, Kume T. J Phys Soc Jpn 1839;1992:61.
[5] Saito S, Hashimoto T. J Chem Phys 2001;114:23.
[6] Saito S, Hashimoto T, Morfin I, Lindner P, Boue F. Macromolecules 2002;35:445.
[7] Kume T, Hattori T, Hashimoto T. Macromolecules 1997;30:427.
[8] Boue F, Lindner P. Europhys Lett 1994;25:421.
[9] Morfin I, Lindner P, Boue F. Macromolecules 1999;32:7208.
[10] Helfand E, Fredrickson GH. Phys Rev Lett 1989;62:2468.
[11] Doi M, Onuki A. J Phys II France 1992;2:1631.
[12] Onuki A, Yamamoto R, Taniguchi T. J Phys II France 1997;7:295.
[13] Onuki A, Yamamoto R, Taniguchi T. Prog Colloid Polym Sci 1997;106:150.
[14] Okuzono T. Mod Phys Lett B 1997;11:379.
[15] Furukawa A, Onuki A. Physica D 2005;205:195.
[16] Takenaka M, Nishitsuji S, Taniguchi T, Yamaguchi M, Tada K, Hashimoto T. Polymer 2006;47:7846.
[17] Nishitsuji S, Takenaka M, Taniguchi T, Hasegawa H. Kobunshi Ronbunshu 2007;64:324.
[18] Ianniruberto G, Marrucci G. J Non-Newtonian Fluid Mech 2000;95:363.
[19] Ianniruberto G, Marrucci G. J Rheol 2001;45:1305.
[20] Ianniruberto G, Marrucci G. J Non-Newtonian Fluid Mech 2002;102:383.
[21] de Gennes PG. J Chem Phys 1980;9:72.
[22] de Gennes PG. Scaling concepts in polymer physics. Ithaca: Cornell University Press; 1979.
[23] Onuki A. J Phys Condens Matter 1997;9:6119.
[24] Binder K. J Chem Phys 1983;79:6387.
[25] Adam M, Delsanti M. J Physique 1984;45:1513.
[26] Osaki K, Inoue T, Uematsu T. J Polym Sci Part B Polym Phys 2000;38:3271.
[27] Osaki K, Inoue T, Uematsu T, Yamashita Y. J Polym Sci Part B Polym Phys 2001;39:1704.
[28] Onuki A. J Phys Soc Jpn 1997;66:1836.
[29] Lees AW, Edwards SF. J Phys C 1972;5:1921.
[30] Naitoh T, Ono S. J Chem Phys 1979;70:4515.
[31] Koga T, Kawasaki K. Phys Rev A 1991;66:1836.
[32] Endoh KM, Saito S, Hashimoto T. Macromolecules 2002;35:7692.
[33] Endoh KM, Takenaka M, Inoue T, Watanabe H, Hashimoto T. J Chem Phys 2008;128:164911.
[34] Saito S, Matsuzaka K, Hashimoto T. Macromolecules 1999;32:4879.